

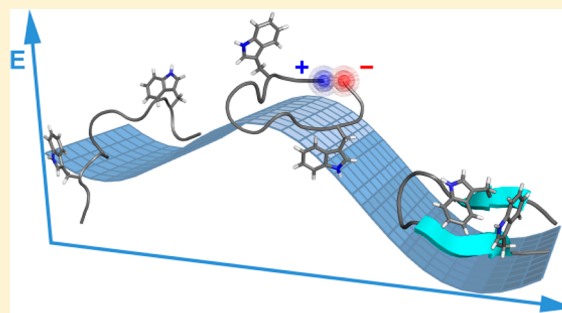
Mutational Effects on the Folding Dynamics of a Minimized Hairpin[†]

Michele Scian, Irene Shu, Katherine A. Olsen, Khalil Hassam, and Niels H. Andersen*

Department of Chemistry, University of Washington, Seattle, Washington 98195, United States

S Supporting Information

ABSTRACT: The fold stabilities and folding dynamics of a series of mutants of a model hairpin, KTW-NPATGK-WTE (HP7), are reported. The parent system and the corresponding DPATGK loop species display submicrosecond folding time constants. The mutational studies revealed that ultrafast folding requires both some prestructuring of the loop and a favorable interaction between the chain termini in the transition state. In the case of YY-DPETGT-WY, another submicrosecond folding species [Davis, C. M., Xiao, S., Raleigh, D. P., and Dyer, R. B. (2012) *J. Am. Chem. Soc.* 134, 14476–14482], a hydrophobic cluster provides the latter. In the case of HP7, the Coulombic interaction between the terminal NH_3^+ and CO_2^- units provides this; a C-terminal Glu to amidated Ala mutation results in a 5-fold retardation of the folding rate. The effects of mutations within the reversing loop indicate the balance between loop flexibility (favoring fast conformational searching) and turn formation in the unfolded state is a major factor in determining the folding dynamics. The -NAAKKX- loops examined display no detectable turn formation propensity in other hairpin constructs but do result in stable analogues of HP7. Peptide KTW-NAAKK-WTE displays the same fold stability as HP7, but both the folding and unfolding time constants are greater by a factor of 20.



The mechanism by which an initially unstructured polypeptide sequence reaches its native structure circumventing the Levinthal paradox¹ is still controversial. It has been suggested that proteins could avoid searching through all possible conformations by taking specific folding pathways. In the diffusion–collision and nucleation models^{2–4} of protein folding, stepwise rapid formation of local secondary structures drives the folding. Hydrophobic collapse followed by the acquisition of secondary structure and tertiary packing interactions is an alternative model.⁵ The structural elements, or “foldons”,^{6,7} that collide and coalesce to form a protein’s tertiary structure must possess the potential to fold to some extent because of strictly local interactions. Helices, local hydrophobic clusters, and β -hairpins are potential foldons. In Dill’s zipping assembly view of protein folding,^{8–10} multiple foldon condensation pathways are proposed to accelerate protein folding, but conformational searching is still the ultimate speed limit¹⁰ of protein folding.

The frequent observation, for β -sheet proteins, that one β -hairpin is formed before or at the folding transition state^{11–20} is evidence of the involvement of a hairpin in nucleation–condensation pathways.^{21–26} As a result, there have been efforts to design β -hairpins for dynamics studies outside of the protein context. Experimental measures of $1/k_F$ for noncyclic β -hairpins at 280–298 K have been in the 0.8–52 μs range;^{27–31} contrarily, faster rates ($1/k_F = 40$ –140 ns) have been reported for three- and four-stranded sheet models.^{32–34} In the case of the faster folding double and triple hairpins, Gai and co-workers^{33,34} have suggested that the rapid folding observed may

reflect multiple pathways to the folded state or downhill folding.

A number of reports have revealed a relationship between the stability of a β -hairpin and the turn forming propensity of the loop region.^{35–38} Moreover, effects of loop length,^{37,39–42} stabilizing cross-strand interactions,^{37,42–48} and attractive Coulombic effects between the oppositely charged chain termini^{49–52} have also been noted. The influence of these factors on folding rates remains incompletely understood. There have been studies that report an increase in folding rate for reversing loop region mutations that increase the “turn propensity”,^{29,30,32–34} but other studies^{28,41} supported a model for β -hairpin folding in which the rate-limiting step is the loop search process required to establish a near-native cross-strand hydrophobic cluster without prior formation of a well-defined native turn. A recent publication⁵³ indicates that a choice between these two mechanisms remains elusive for a hairpin with a topology similar to that of the peptides reported herein.

Analogues of the C-terminal hairpin (GB1p) of the B1 domain of protein G,^{54,55} including “trpzip” hairpins,⁵⁶ have played a prominent role in hairpin dynamics studies.^{28,29,57} Indeed, fluorescence-monitored T-jump experiments⁵⁷ with GB1p were the basis for the original hairpin zipper folding mechanism. Our nuclear magnetic resonance (NMR) relaxation studies²⁸ revised $1/k_F$ at 298 K for GB1p from 6 to 20 μs , in large part, as a result of a change in the estimated folding

Received: February 5, 2013

Revised: March 21, 2013

Published: March 22, 2013



equilibrium constant. Recalculating the fluorescence-monitored T-jump data using our K_F value brings the two folding time measures ($1/k_F$) within experimental error ($\pm 2 \mu\text{s}$). The folding dynamics data for GB1p and related peptides are listed in Table 1.

Table 1. Representative Dynamics Data for GB1 Hairpin Analogues at $297 \pm 3 \text{ K}$

		k_F ($\times 10^3 \text{ s}^{-1}$)	k_U ($\times 10^3 \text{ s}^{-1}$) at 298 K
GB1p	GE WTY-DDATKT-FTV TE	51	179
	D7P	110	90
	K10G	390	780
GB1m2	GE WTY-NPATGK-FTV TE	260	156
GB1m3	KK WTY-NPATGK-FTV QE	520	220
trpzip4	GE WTW-DDATKT-WTW TE-NH ₂	67	4.3 (ref 36)
HP7	KTW-NPATGK-WTE	1800	210 (this study)
CLN025	YY-DPETGT-WY	5200	200 (ref 53)

Loop optimization (GB1m2 vs GB1p) increases the stability of the hairpin fold by 4.5 kJ/mol,⁵¹ this result arising exclusively from an increased folding rate. On the basis of data reported by Du et al.,²⁹ the even larger fold stability increase ($\geq 7.5 \text{ kJ/mol}$) associated with Trp/Trp interactions in trpzip4 is largely a reflection of retarded unfolding rather than an increase in the folding rate constant. Two loop mutations (D7P and K10G), each of which increases fold stability, have quite different effects on folding dynamics: the D7P mutation increases k_F and decreases k_U ,²⁸ while the K10G mutation increases both rates dramatically.⁵⁸ It would appear that loop configurational entropy considerations (e.g., Gly vs Pro content changes), rather than just changes in the net thermodynamic stability, can be a factor in hairpin dynamics. The GB1m3 versus GB1m2 comparison in Table 1 indicates that the hairpin stabilization associated with replacing a repulsive Coulombic interaction near the chain termini (E2/E16) with attractive K/E interactions is largely the result of a 2-fold increase in the folding rate. Given the remoteness from the turn loci, we suggested²⁸ that this was difficult to rationalize by a “zippering” from the turn mechanism of hairpin folding. Subsequent studies have confirmed hairpin stability enhancement caused by attractive Coulombic interactions between the charges at the extreme termini of this series of peptides.⁵² The last entry in Table 1, CLN025, is a peptide with the same turn geometry that has been reported to be an ultrafast folding system.⁵³ In the CLN025 study, it was concluded that neither the zipper mechanism nor the hydrophobic collapse mechanism could completely rationalize the result and it was suggested that hydrophobic interactions between the terminal aromatic groups lead to a precollapsed structure. In this account, we present hairpin dynamics data from NMR relaxation measurements^{28,59–62} for a wide range of strand-terminal and loop mutations of peptide HP7⁶³ to elucidate the hairpin formation pathways. Mutations at the chain termini and a wide range of mutations in the NPATGK loop, which dramatically altered the loop entropy, are tolerated and do not alter the folded state geometry. These mutations do alter the folding equilibrium and provide, as a result, measures of the effects of both loop and strand mutations on fold stability as well as folding and unfolding rates.

EXPERIMENTAL PROCEDURES

Materials. With the exception of (E12A-NH₂)-HP7, the analogues were synthesized on an Applied Biosystems 433A synthesizer employing standard Fmoc solid-phase peptide synthesis methods. Wang resin preloaded with the C-terminal amino acid in the synthesis provided an unprotected C-terminus upon cleavage. HP7 (KTW-NPATGK-WTE) analogues prepared specifically for this study replaced NPATGK with NGATGK, NPGTGK, NGGTGK, NAAAGK, NAAAKT, NAAAKK, and NAAAKG. For (E12A-NH₂)-HP7, a Rink amide resin provided a C-terminal amide function upon cleavage.

Additional peptides were prepared to ascertain, in other hairpin contexts, the turn propensities of NPATGK, NAAAGK, and NAAAKK with and without the turn-flanking Trp residues. These included KKLWVS-NPATGK-KIWVSA and KKLWVS-NAAAKK-KIWVSA. Fold stability data for these and other constructs appear in the Supporting Information.

Peptides were cleaved using 95% trifluoroacetic acid (TFA), with 2.5% triisopropylsilane (TIS) and 2.5% water. The cleavage product was then purified using reverse-phase high-performance liquid chromatography (HPLC) on a Varian C₁₈ preparatory-scale column with a water (0.1% TFA)/acetonitrile (0.085% TFA) gradient. Collected fractions were then lyophilized and their identity and molecular weight confirmed on a Bruker Esquire ion trap mass spectrometer. In some cases, an additional HPLC purification using a C₈ column with a water (0.1% TFA)/acetonitrile (0.085% TFA) gradient or a C₄ column with a water (0.1% TFA)/methanol (0.085% TFA) gradient was required to obtain peptide samples meeting our purity criteria by NMR analysis. All the other HP7 mutants were available from previous studies;⁶³ these were repurified prior to an additional determination of the circular dichroism (CD) and NMR melts as well as NMR line widths. The structures were fully supported by mass spectrometry, with the NMR assignments confirming the sequence and purity. The thermodynamic stability data from CD and NMR studies of the HP7-related peptides are listed in Table S1 of the Supporting Information.

NMR Spectroscopy. All NMR spectra were recorded on a Bruker DRX-500 or DMX-750 spectrometer. Peptide resonances were assigned through a combination of two-dimensional (2D) TOCSY and NOESY experiments with WATERGATE⁶⁴ solvent suppression. The former employed a 60 ms MLEV-17 spin lock⁶⁵ and the latter a 150 ms mixing time. The samples for 2D spectra consisted of 1–1.5 mM peptide in buffered water [20 or 50 mM phosphate buffer (pH 6.0)] with 10% D₂O. Sodium 2,2-dimethyl-2-silapentane-5-sulfonate (DSS) was used as the internal chemical shift reference and set to 0 ppm under all conditions independent of temperature and phosphate buffer concentration.

For NMR line width studies and additional melting data, the peptides were deuterium-exchanged by repeated lyophilization from D₂O and ¹H one-dimensional spectra (512 scans acquired at a resolution of 32K and 64K points for the 500 and 750 MHz spectrometers, respectively) were recorded with 0.6–1 mM peptide concentrations in 20 or 50 mM phosphate-buffered 99.9% D₂O (pH 6.0).

Folding–Unfolding Equilibrium Measurements. Diagnostics of folding for peptide HP7 have already been defined. Expectations based on the pattern of backbone CSD values for hairpins⁶⁶ are that the ($S \pm \text{even}$) H α and the ($S \pm \text{odd}$) H_N

should be downfield by ~ 1 ppm at 100% folding (see Figure 1 for the labeling scheme); in HP7, a number of these are

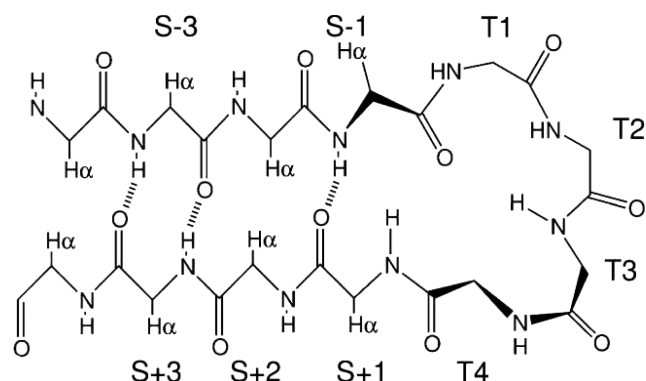


Figure 1. Nomenclature for HP7-related hairpins.

modified by ring current effects. It has also been established that the [4:6]-hairpin loop has diagnostic CSDs, upfield shifts for G8 α (T4), T3H α , and (S + 1) H α . On the basis of the folding thermodynamics parameters for HP7,⁶³ the CSD_{100%} values for these and key sites that experience ring current shifts have been established. These are detailed in the Supporting Information.

Extracting Folding–Unfolding Rate Constants from Exchange Broadening Data. This NMR method relies on the measurement of exchange broadening (Δ^{ex}). In the case of folded–unfolded state exchanges that occur in the $<100 \mu\text{s}$ range, where the probe signal will occur at the population-averaged chemical shift, the relationship among the line width (Δ^{obs}), the exchange rates, and the chemical shift difference ($\Delta\nu$) between the states is given by eq 1

$$\Delta^{\text{ex}} = \Delta^{\text{obs}} - \Delta^0 = 4\pi\tau_{\text{ex}}\chi_{\text{F}}\chi_{\text{U}}(\Delta\nu)^2 \quad (1)$$

where χ_{F} is the mole fraction of the folded state ($K_{\text{F}} = \chi_{\text{F}}/\chi_{\text{U}}$), Δ^0 is the “intrinsic” line width expected in the absence of exchange broadening, and $\tau_{\text{ex}} = (k_{\text{F}} + k_{\text{U}})^{-1}$.

For hairpins and other peptide folds that are incompletely populated under accessible conditions, defining fully folded structuring shifts (CSD_{100%}) and whether they may have some residual temperature dependence stands as the greatest potential source of error in dynamic NMR folding rate determinations. Once these have been defined, however, the NMR method has the distinct advantage that the equilibrium constant at any temperature can be derived from the observed chemical shift for the probe (eq 2).

$$\chi_{\text{F}} = (\delta_{\text{obs}} - \delta_{\text{coil}})/\text{CSD}_{100\%} \quad (2)$$

Further details concerning how we extract Δ^{ex} from line shape differences between two first-order doublets with the same coupling constant have been published previously,²⁸ and their specific implementation in this case appears in the Supporting Information.

Measurements at two field strengths provide a test of an inherent assumption in the method, that Δ^{ex} can be attributed exclusively to exchange broadening caused by the folded/unfolded equilibrium. Exchange broadening due to this mechanism should be proportional to $(\Delta\nu)^2$; thus, the calculated Δ^{ex} should be 2.25 times larger at 750 MHz than at 500 MHz. For Δ^{ex} values of >1.2 Hz at 500 MHz, this condition is met within experimental error (Table S3 of the

Supporting Information). When Δ^{ex} is small (<2.5 Hz at 750 MHz), we employ only the value determined at 750 MHz for rate calculations.

Folding rate constants are derived using eq 3. With the folding equilibrium constant established, this also provides the unfolding rate.

$$k_{\text{F}} = 4\pi\chi_{\text{U}}(\chi_{\text{F}})^2(\Delta\nu)^2(\Delta^{\text{ex}})^{-1} \quad (3)$$

Equation 3, which applies near the fast exchange limit, was reported in 1959 by Piette and Anderson⁶⁷ and applied to hairpin dynamics⁶⁸ in 1999, when it was used to extract upper limits for three-stranded sheet formation time scales. We have previously established the conditions required for the application of eq 3;²⁸ all of the systems examined herein meet those conditions. To obtain error estimates for k_{F} , we use χ_{U} values based on alternative CSD values, one based on a single common value for the chemical shift of the Trp H ϵ 3 probe in the folded state independent of loop mutations, and two others based on the CSD_{100%} values (and δ_{F} temperature dependencies) derived from Table S1 of the Supporting Information.

RESULTS

The backbone conformation and the particular edge-to-face (EtF) packing motif of the indole rings in the turn-flanking Trp residues observed in the β -hairpins examined herein are shown in Figure 2. The EtF aromatic interaction results in a dramatic

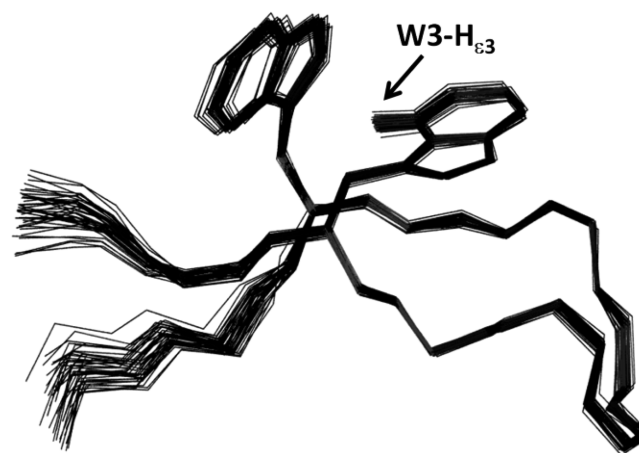


Figure 2. Packing motif for the turn-flanking indole rings (Trp3 and Trp10) and the backbone conformation of HP7.⁶³ The W3–H ϵ 3 location is highlighted.

(>2.2 ppm) upfield structuring shift for the N-terminal Trp H ϵ 3 resonance (W3–H ϵ 3) due to the ring current effects of the other Trp. The line widths of this shifted resonance provide the dynamics data.

The H ϵ 3 resonance of the Trp at the C-terminus experiences virtually no structuring shift and, thus, is an ideal internal reference for establishing intrinsic broadening effects (Δ^0). We observe significant differential broadening at the upfield-shifted W3–H ϵ 3 resonance of hairpins with this motif (see Figure 3, vide infra).

Verification of two-state folding and accurate $\Delta\nu$ values are the key requirements for extracting meaningful rates by the NMR line width method we employ. The use of several local probes represents a stringent test for two-state folding. Chemical shifts provide a powerful tool for detecting partially

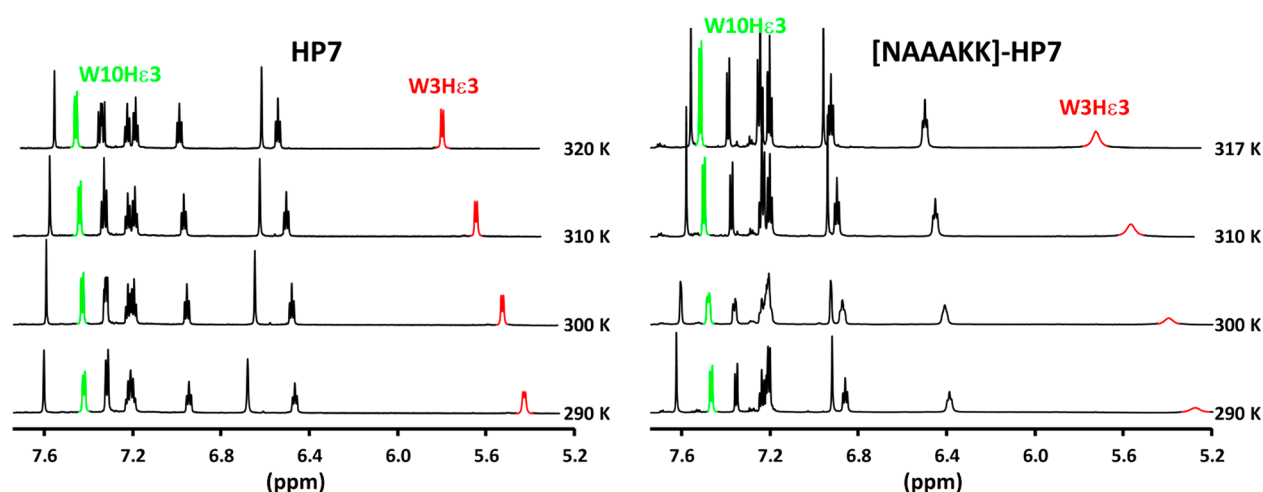


Figure 3. Aromatic region of 750 MHz NMR spectra of HP7 and a loop region mutant in D₂O (pD 6.5). The colored peaks are the Hε3 resonances of the two Trp indole rings: red for W3 and green for W10 (which served as the control for no exchange broadening). Even though the NAAAKK loop mutant displays a somewhat larger upfield shift for W3-Hε3 and a comparable shift melt, the extensive line broadening indicates much slower folding dynamics.

folded states under equilibrium melting conditions. For non-two-state melting behavior, some sequence segments of the peptide would be expected to show structuring shifts (native-like or reflecting an alternative structure), while others would be in a statistical coil conformation, leading to different local melting curves depending on the probe location.^{28,41,66,69,70} We employed eight backbone proton sites for measuring the fraction folded values (χ_F) of the hairpins. Five of these monitor β -strand alignment; the other three indicate the extent of turn formation. The agreement between these folding measures for distinct substructural elements supports a two-state unfolding mechanism for all of the species examined (Supporting Information). The melting curves for each of these proton sites revealed that all of them displayed the same fractional degree of unfolding on warming, strong evidence against the formation of partially melted intermediates and a downhill folding scenario.

Because the upfield W3-Hε3 resonance provides both the shift data giving the extent of folding (χ_F) and the line widths that afford the folding dynamics, the accuracy of the extrapolated 100% folded shift value for this site (and its temperature dependence) in each peptide was a major concern. The extrapolated 100% folded CSDs at 280 K for the HP7 series of peptides ranged from -2.39 to -2.64 ppm (Supporting Information). As has been observed in other studies,^{71–73} Hε3 ring current shifts in cross-strand Trp/Trp units decrease at higher temperatures. This was incorporated in our dynamics analysis as a temperature-dependent value for the fully folded chemical shift of W3-Hε3. For this set of analogues, two values were required for the analysis: $\delta_F = 5.15 + 0.004(T - 280)$, or $\delta_F = 4.98 + 0.005(T - 280)$. The latter applied to analogues with extensive mutations in the NPATGK loop. Chemical shift melting curves of the W3-Hε3 resonance for all of the peptides in D₂O (the medium employed for the NMR line shape analyses) that support the use of these equations appear in Figures S1 and S2 of the Supporting Information.

One advantage of using the chemical shift as a probe of folding is that this method is insensitive to partial aggregation of the sample at elevated temperatures, a common problem in thermal denaturation studies. Aggregation dynamics are much slower than conformer interconversion with the broad signals

for the aggregate not averaged in with those of the monomeric state. However, even under these conditions, the monomer–aggregate interconversion can result in broadening of the monomer signals, but the resulting line width increment due to exchange with an aggregate does not scale with $\Delta\nu$. Rapid exchange between the monomeric folded state and the unfolded ensemble will result in Δ^{ex} values that are proportional to $(\Delta\nu)^2$ and, thus, to (field strength)². In every case, the Δ^{ex} ratio values derived for HP7 analogues at 500 and 750 MHz are as expected (2.25): 2.33 ± 0.20 ($n = 24$) (see Table S5 of the Supporting Information).

The resonances for the two Trp Hε3 sites were resolved in all of the analogues examined, with only the upfield W3 site displaying line broadening. Figure 3 illustrates a large difference in Hε3 line widths observed for two HP7 systems that have essentially the same fold stability and very similar melting behavior.

For dynamics analyses, we always assumed the same coil value (7.58 ppm) for Trp Hε3 but employed the alternative temperature-dependent δ_{folded} values given above. In an alternate analysis, we assumed a common δ_{folded} values of 5.10 ppm, independent of loop residue or mutations in the chain termini. As a rule, the Arrhenius plots derived using the temperature-dependent CSD_{100%} value provided a more nearly linear plot for $\ln k_U$. The key fold stabilities (as ΔG_U) and folding and unfolding rates appear in Table 2. Table S2 (Supporting Information) provides data at additional temperatures, complementary data measured at 500 MHz, and includes the χ_F value for each entry.

Accurate dynamics data are available over a 6 kJ/mol range ($\Delta\Delta G_U$) of fold stabilities at 300 K. The range of both folding and unfolding rates is larger, 9 kJ/mol in $RT(\ln k)$ units; throughout, Arrhenius behavior is observed. In all cases, the plot of $\ln k_U$ versus reciprocal temperature is linear within experimental error. The slopes of the Arrhenius plots for k_U are quite similar, reflecting a 2.5 ± 0.2 -fold rate increase for a 10 °C temperature increment. Representative Arrhenius plots appear in Figure 4 and the Supporting Information. For examining the correlation between thermodynamic stability and dynamics effects of mutations, we compare $\Delta\Delta G_U$ and $\Delta(\ln k)$; these are

Table 2. Effects of HP7 Mutations on Folding and Unfolding Rates in D₂O^a

mutation	temp (K)	ΔG_U (kJ/mol)	$\ln k_F$	$\ln k_U$
none (KTW-NPATGK-WTE)	290	5.8	13.7 ± 0.2	11.3 ± 0.2
	300	5.4	14.60	12.46
	320	3.7	15.71	14.31
strand mutations				
K1A, E12A ^b	300	3.0	14.33	13.11
E12A-NH ₂ ^b	290	3.1	12.54	11.26
	300	1.85	13.02	12.28
	310	0.46	13.33	13.15
loop mutations of NPATGK				
DPATGK ^b	300	4.2	14.86	13.18
APATGK ^c	300	−0.95	nd ^f	nd ^f
NAATGK	300	4.6	14.28	12.41
NPAAGK	300 ^d	4.2	13.6 ± 0.3	11.9 ± 0.3
NAAAGK	300 ^d	6.0	13.1 ± 0.2	10.7 ± 0.2
NAAAKG	300	1.9	12.18	11.42
NAAAKK	300	5.3	11.60	9.47
	310	4.4	12.03	10.34
	317	3.5	12.30	10.97
NAAAKT	300	4.1	11.69	10.05
	320	1.9	12.52	11.81
	at pH 3	300 ^e	0.81	10.63
	315 ^e	−1.1	11.69	12.08
NPATAK	300	3.8	12.6	11.07
NPGTGK	300	3.3	13.7	12.4
NGATGK	280 ^d	4.6	12.13	10.16
	290	4.0	12.51	10.86
NGATGK	300 ^d	2.9	12.88	11.73
NGGTGK	280 ^d	2.6	11.24	10.1
	300 ^d	0.17	12.1	12.03
	320 ^d	−2.9	12.6	13.7

^aData recorded at nominal pH 6 (750 MHz proton observation) unless otherwise specified. The temperature-dependent value used for the fully folded chemical shift of W3-H ϵ 3 (δ_F) was $4.98 + 0.005(T - 280)$ except as noted. The results using a common temperature invariant 100% folded value (5.10 ppm) are listed in Table S4 of the Supporting Information. ^bA δ_F equal to $5.15 + 0.004(T - 280)$ was used for HP7 and related species. ^cStability data from ref 63; dynamics data not available for the same sample. ^dMeasurement taken at 500 MHz. ^eMeasurement taken at pH 3. ^fNot determined.

listed for single-site loop mutations in Table S3 of the Supporting Information.

DISCUSSION

The NPATGK loop of HP7 was based⁵¹ on location-specific residue statistics for [4:6]-hairpins in proteins. This sequence has subsequently been successfully employed in a number of hairpin and three-stranded constructs.^{66,74} A similar analysis led Honda and co-workers to the DPETGT turn sequence that appears in chignolin⁷⁵ and further optimized hairpins.⁷⁶ This study serves to confirm that the key features of this turn sequence are aryl-Asx-XXXGX-aryl, with the flanking aromatic residues providing significant stability. This is borne out by the effects of single-site residue mutations within this sequence in HP7 analogues (Table S3 of the Supporting Information); an N4A mutation was highly destabilizing (folding rates could not be determined), with the G8A mutation having the largest

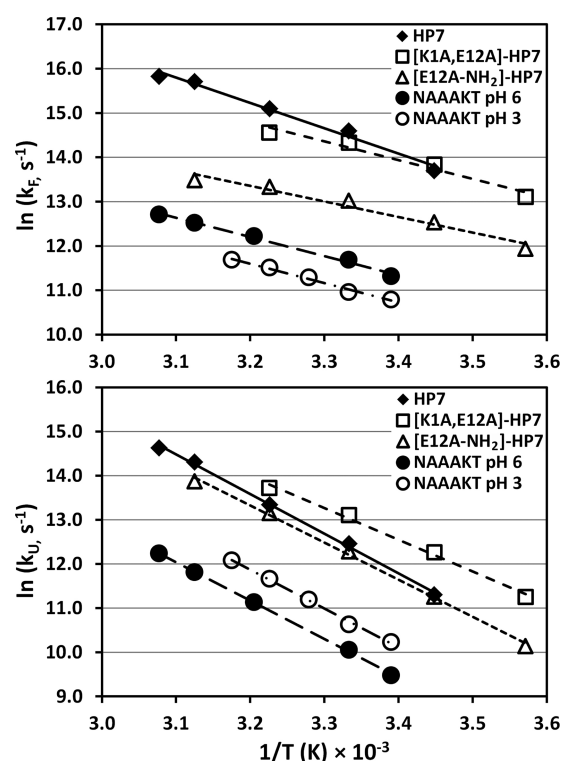


Figure 4. Arrhenius plots for HP7 (◆), [K1A,E12A]-HP7 (□), [E12A-NH₂]-HP7 (△), and the NAAAKT loop analogue at pH 6 (●) and pH 3 (○). The folding rate constants appear in the top panel. The unfolding rate constants appear in the bottom panel. All lines are least-squares fits.

effect on the folding rate (a 7-fold retardation), with a smaller reduction observed for k_U . These results were, to some extent, expected because G8 has ϕ and ψ values of 94° and 47° , respectively, in the HP7 NMR structural ensemble.⁶³ In the case of the NAAAKK loop mutant, we examined the effect of non-native versus native introduction of glycine: NAAAKK \rightarrow NAAAKG ($\Delta\Delta G_U = -3.4$ kJ/mol, $\Delta\ln k_F = 0.6$, $\Delta\ln k_U = 2.0$) versus NAAAKK \rightarrow NAAAGK ($\Delta\Delta G_U = 0.7$ kJ/mol, $\Delta\ln k_F = 1.5$, $\Delta\ln k_U = 1.2$). The introduction of glycines at positions other than the “native” one (G8) is destabilizing and results in enhanced melting, but the effects on the dynamics are not uniform (Table S3 of the Supporting Information). In the case of the NAAAKK \rightarrow NAAAKG mutation, the glycine insertion increases both the folding and unfolding rate (see Figure S6 of the Supporting Information). With a decrease in ΔG_U in this case, the accelerated folding can, in our opinion, be attributed only to a more rapid conformational search for the fold-stabilizing indole/indole geometry at the ends of a more flexible loop upon introduction of a Gly unit.

Turning to the specific questions raised in the introduction concerning the factors that govern hairpin formation rates, we find the HP7 analogue data presented here provide insights into three features: (1) the effects of Coulombic interactions near the chain termini, (2) the correlation between folding rates and thermodynamic stability, and (3) the effects of loop flexibility versus intrinsic conformational preferences. Arrhenius plot comparisons (Figures 4) provide data regarding the Coulombic effect; these probe the effects of the interaction of both oppositely charged side chains near the chain termini and of the N-terminal NH₃⁺ and the C-terminal backbone carboxylate on fold stability and dynamics.

There are also many examples in the literature^{45–50,63} in which C-terminal carboxylate protonation reduces hairpin fold stability. In this study, we examined the effects on folding dynamics in the case of the NAAAKT loop mutant. Carboxylate protonation, as for other HP7 analogues,⁶³ is destabilizing with a 2-fold decrease in the folding rate constant and an acceleration of unfolding.

The chain terminal [K1A,E12A]-HP7 and [E12A-NH₂]-HP7 mutations probe the effects of the interaction of both oppositely charged side chains near the chain termini and of the N-terminal NH₃⁺ and the C-terminal backbone carboxylate on fold stability and dynamics. Replacing the N-terminal Lys and the C-terminal Glu with alanine does not alter the folding rate; the slight decrease in thermodynamic stability associated with this change is due to somewhat accelerated unfolding. This analogue retains the attractive interaction between the backbone NH₃⁺ and C-terminal CO₂⁻ units. In contrast, replacing the C-terminal Glu with amidated alanine, which removes this interaction, results in a significant (5-fold) decrease in the folding rate with essentially no change in the unfolding rate constant. This comparison suggests that the fold-favoring Coulombic effect reflects folding acceleration due to the charges at the backbone termini with less contribution from oppositely charged side chain functions. There are cases in the literature^{52,63} in which N-terminal acetylation has been demonstrated to decrease hairpin fold stability. These may reflect the same phenomenon.

Substantial folding rate acceleration due to an attractive Coulombic interaction between the extreme termini of the structure would require, with a zippering from the turn mechanism, a late transition state with nearly complete hairpin formation. The alternative is a collapsed structure including Coulombic association between the termini as an early intermediate in folding with cross-strand H-bonding and the formation of the stabilizing turn-flanking Trp/Trp interactions as somewhat later events in the folding pathway.

Turning to the second question, the correlation between folding rates and thermodynamic stability, this has been studied extensively in other systems, particularly proteins. A common feature observed in prior reports of hairpin dynamics comparisons over turn replacements and turn site mutations has been an increased folding rate for turn sequences with an enhanced turn forming propensity.^{29,30} With the extensive studies of replacements of the SRSSGR reversing loop in the Pin1 WW domain by Kelly and Gruebele,^{77–79} this conclusion has been extended to protein contexts. Among the single-site mutations we examined, NAATGK → NAAAGK ($\Delta\Delta G_U = 1.7$ kJ/mol, $\Delta\ln k_F = -1.2$, and $\Delta\ln k_U = -1.7$) is a clear exception to this expected correlation. Slow folding, coupled with surprisingly high thermodynamic stability, was observed for all of the NAAAXX loop species examined. For the NP⁵AT⁷GK reversing loop, the P5A and T7A mutations each decreased fold stability and the folding rate constant; the double mutation resulted in a folding rate retardation that was slightly greater than the sum of the effects of the two individual mutations, but this was coupled with significant fold stabilization. The NAAAKK loop species is the slowest folding species examined, even though it has the same fold stability as the “optimized” NPATGK loop species (HP7). The NMR spectra that provided the folding dynamics for these two species appear in Figure 3. At 300 K, both are 89 ± 1% folded in D₂O; the exchange broadening observed is 1.7 and 34 Hz (at 750 MHz),

respectively, corresponding to a 20-fold difference in both the folding and unfolding rates constants.

To explore potential differences between the optimized NPATGK reversing loop and the NAAAXX loops, we examined them as a replacement for β -turn sequences [e.g., XNGK and X-(D-Pro)-GK, where X is S,V, or I] in hairpins and three-stranded sheet models with and without the turn-flanking Trp/Trp pair (see the Supporting Information). A turn-flanking aryl/aryl pair, also a feature of the GB1 peptide,^{54–56} is important for high fold stability with both sequences. However, the NAAAKK (and other NAAAXX) sequence cannot replace favorable β -turns in the absence of the flanking aryl/aryl pair, while the NPATGK sequence does appear to have an “intrinsic” chain reversing propensity.^{74,80}

Turning to loop search and stiffness considerations, loop contact time studies have established that Pro has the most dramatic rate retarding effect in loop conformational searches while the increased flexibility of Gly can decrease loop-end contact times.^{81,82} With the NPATGK loop sequence, however, a significant level of loop prestructuring may occur. Loop mutants with the PATG sequence replaced by AAAK should display comparable flexibility, but turnlike conformations appear to be less significant contributors to the unfolded ensemble for the AAAK species. Thus, with both Pro and Gly at their preferred locations in the loop sequence, the folding direction is favored by loop prestructuring. The observation that unfolding is retarded by the PATG → AAAK change to the same extent as folding suggests that unfolding proceeds through an enthalpically unfavorable loop conformation for the NAAAK species. For this series of hairpins, there is no apparent correlation between fold stability and the rate of fold formation; rather, the data support a role for loop conformational search requirements, including loop flexibility, and the extent to which prestructuring of the loop is favored by the sequence.

How do these new observations regarding hairpin dynamics fit within the context of other literature observations and current questions concerning protein folding mechanisms? Given the close structural analogies between the HP7 hairpins and CLN025 (YY-DPETGT-WY; $T_m = 70$ °C), this is the first comparison considered here. Although the authors reported⁵³ the CLN025 dynamics data as relaxation rates rather than specific k_F and k_U values, folding equilibrium constants were also reported; these allow a calculation of $1/k_F$ values of ~190 ns (298 K) and ~115 ns (318 K). The fastest folding times we observed for our DPATGK and NPATGK loop species ($1/k_F$) were 530 ns (300 K) and 150 ns (320 K). All of these folding times are faster than the expected^{53,83,84} 1 μ s speed limit for hairpin formation.

There are some distinctions between the dynamics data for CLN025 and the HP7 analogues. CLN025 displayed a break at 308 K in both the van't Hoff melt analysis and the Arrhenius plot for $\ln k_R$ with probe-dependent kinetics observed in the high-temperature region. In the Arrhenius plot, this corresponds to a radically decreased slope at temperatures above the break point, suggesting either no or a very small (<10 kJ/mol) activation energy. Some of the HP7 analogues display a flattening of the Arrhenius plot for $\ln k_F$; however, we did not extend the studies to sufficiently high temperatures to ascertain whether there are two distinct folding regimes because other evidence suggested that aggregation becomes a competing process at higher temperatures. The unfolding activation energies (E_a) for HP7 analogues are relatively constant (69 ±

6 kJ/mol). The E_a values derived from the linear fits to the Arrhenius plots for folding rates in Figure 4 and Figure S6 of the Supporting Information range from 30 to 50 kJ/mol, values that bracket the ~ 45 kJ/mol value observed for the low-temperature portion of the CLN025 Arrhenius plot. The fastest folding system (the NPATGK loop with “wild-type” strands) has the largest activation energy (~ 50 kJ/mol) in the folding direction. We view this, in the case of the HP7 systems, as the barrier for an essentially two-state folding process that includes the formation of the Trp/Trp EtF interaction and some cross-strand H-bonds within a short antiparallel β -sheet. CLN025 also has an EtF aryl/aryl pair (Y2/W9), but these side chains, in combination with Y1 and Y10, may represent hydrophobic capping of a turn rather than two-residue β -strands. This may reduce the extent to which CLN025 is an appropriate model for hairpin folding.

Given the observation of probe-dependent dynamics for CLN025,⁵³ it will be essential to ascertain whether this is also the case for the HP7 hairpins. Efforts to provide this information are in progress. To date, Trp fluorescence-monitored T -jump studies (15–26 °C) have confirmed the ultrafast folding of the NPATGK loop species, the folding rate retardation associated with the C-terminal Glu to Ala-NH₂ mutation, the slow folding of the NGGTGK loop species, and the even slower folding of two NAAAKX loop species. Because Trp fluorescence changes may reflect the same structuring transition that determines the ring current shifts used in NMR dynamics, the synthesis of systems with ¹³C=O labels at sites that monitor specific H-bond formation within the reversing loops and between the β -strands for T -jump experiments is in progress. These should provide the additional probes needed to ascertain whether there is sequential formation of different structural elements (or strict two-state folding) for these hairpin models. However, it is already apparent that this series of HP7 analogues has provided evidence that ultrafast hairpin formation requires both some prestructuring of the loop and favorable Coulombic interactions between the chain termini. The latter is provided by the backbone NH₃⁺ and CO₂[−] groups. The NPATGK sequence results in loop prestructuring, while a variety of NAAAKX sequences do not, even though stable hairpins result with all of these loop sequences. We anticipate that these sequences in hairpins stabilized with β -capping units at the ends of longer β -strands will provide additional insights into the contribution of loop conformational search times to β -hairpin formation.

■ ASSOCIATED CONTENT

■ Supporting Information

More detailed descriptions of methods, fold populations (χ_F) derived from NMR shifts (Table S1), folding and unfolding rates obtained using a single temperature invariant δ_{folded} value of W3-H ϵ 3 (Table S4) and a temperature-dependent δ_{folded} (Table S2), exchange broadenings measured at 500 and 750 MHz (Table S5), correlations between mutational thermodynamic and dynamics changes (Table S3 and Figures S4 and S5), and chemical shift melting curves (Figure S1 and S2) for some of the peptides examined. This material is available free of charge via the Internet at <http://pubs.acs.org>.

■ AUTHOR INFORMATION

Corresponding Author

*Telephone: (206) 543-7099. E-mail: andersen@chem.washington.edu.

Funding

This work was supported by grants from the National Science Foundation (CHE0650318 and CHE1152218). M.S. received salary as a postdoctoral research associate on National Institutes of Health Grant GM059658 during some of these studies.

Notes

The authors declare no competing financial interest.

■ ACKNOWLEDGMENTS

We thank Gurusamy Balakrishnan for providing fluorescence-monitored T -jump data for a number of HP7 analogues that served to validate the NMR line shape dynamics.

■ ADDITIONAL NOTE

[†]This is the second paper in the series Elucidating Polypeptide Folding Dynamics by ¹H NMR; the first paper of the series is ref 28.

■ REFERENCES

- (1) Levinthal, C. (1969) in *Mossbauer Spectroscopy in Biological Systems* (Debrunner, P., Tsibris, J. C. M., and Munch, E., Eds.) pp 22–24, University of Illinois, Monticello, IL.
- (2) Karplus, M., and Weaver, D. L. (1976) Protein-folding dynamics. *Nature* 260, 404–406.
- (3) Wetlaufer, D. B. (1973) Nucleation, rapid folding, and globular intrachain regions in proteins. *Proc. Natl. Acad. Sci. U.S.A.* 70, 697–701.
- (4) Daggett, V., and Fersht, A. R. (2003) Is there a unifying mechanism for protein folding? *Trends Biochem. Sci.* 28, 18–25.
- (5) Ptitsyn, O. B. (1987) Protein Folding: Hypotheses and Experiments. *J. Protein Chem.* 6, 273–293.
- (6) Dill, K. A., Fiebig, K. M., and Chan, H. S. (1993) Cooperativity in protein-folding kinetics. *Proc. Natl. Acad. Sci. U.S.A.* 90, 1942–1946.
- (7) Panchenko, A. R., Luthey-Schulten, Z., and Wolynes, P. G. (1996) Foldons, protein structural modules, and exons. *Proc. Natl. Acad. Sci. U.S.A.* 93, 2008–2013.
- (8) Dill, K. A., Ozkan, S. B., Weikl, T. R., Chodera, J. D., and Voelz, V. A. (2007) The protein folding problem: When will it be solved? *Curr. Opin. Struct. Biol.* 17, 342–346.
- (9) Voelz, V. A., and Dill, K. A. (2007) Exploring zipping and assembly as a protein folding principle. *Proteins* 66, 877–888.
- (10) Ghosh, K., Ozkan, S. B., and Dill, K. A. (2007) The ultimate speed limit to protein folding is conformational searching. *J. Am. Chem. Soc.* 129, 11920–11927.
- (11) Matheson, R. R., and Scheraga, H. A. (1978) Method for Predicting Nucleation Sites for Protein Folding Based on Hydrophobic Contacts. *Macromolecules* 11, 819–829.
- (12) Grantcharova, V. P., Riddle, D. S., Santiago, J. V., and Baker, D. (1998) Important role of hydrogen bonds in the structurally polarized transition state for folding of the src SH3 domain. *Nat. Struct. Biol.* 5, 714–720.
- (13) Grantcharova, V. P., Riddle, D. S., and Baker, D. (2000) Long-range order in the src SH3 folding transition state. *Proc. Natl. Acad. Sci. U.S.A.* 97, 7084–7089.
- (14) Martinez, J. C., and Serrano, L. (1999) The folding transition state between SH3 domains is conformationally restricted and evolutionarily conserved. *Nat. Struct. Biol.* 6, 1010–1016.
- (15) Kortemme, T., Kelly, M. J., Kay, L. E., Forman-Kay, J., and Serrano, L. (2000) Similarities between the spectrin SH3 domain denatured state and its folding transition state. *J. Mol. Biol.* 297, 1217–1229.
- (16) Walkenhorst, W. F., Edwards, J. A., Markley, J. L., and Roder, H. (2002) Early formation of a β -hairpin during folding of staphylococcal nuclease H124L as detected by pulsed hydrogen exchange. *Protein Sci.* 11, 82–91.
- (17) Gruebele, M., and Wolynes, P. G. (1998) Satisfying turns in folding transitions. *Nat. Struct. Biol.* 5, 662–665.

- (18) Martinez, J. C., Pisabarro, M. T., and Serrano, L. (1998) Obligatory steps in protein folding and the conformational diversity of the transition state. *Nat. Struct. Biol.* 5, 721–729.
- (19) Guo, Z. Y., and Thirumalai, D. (1995) Kinetics of Protein-Folding: Nucleation Mechanism, Time Scales, and Pathways. *Biopolymers* 36, 83–102.
- (20) McCallister, E. L., Alm, E., and Baker, D. (2000) Critical role of β -hairpin formation in protein G folding. *Nat. Struct. Biol.* 7, 669–673.
- (21) Bofill, R., Simpson, E. R., Platt, G. W., Crespo, M. D., and Searle, M. S. (2005) Extending the folding nucleus of ubiquitin with an independently folding β -hairpin finger: Hurdles to rapid folding arising from the stabilisation of local interactions. *J. Mol. Biol.* 349, 205–221.
- (22) Went, H. M., and Jackson, S. E. (2005) Ubiquitin folds through a highly polarized transition state. *Protein Eng., Des. Sel.* 18, 229–237.
- (23) Gu, H., Kim, D., and Baker, D. (1997) Contrasting roles for symmetrically disposed β -turns in the folding of a small protein. *J. Mol. Biol.* 274, 588–596.
- (24) Riddle, D. S., Grantcharova, V. P., Santiago, J. V., Alm, E., Ruczinski, I., and Baker, D. (1999) Experiment and theory highlight role of native state topology in SH3 folding. *Nat. Struct. Biol.* 6, 1016–1024.
- (25) Fersht, A. R. (1993) The sixth Datta Lecture. Protein folding and stability: The pathway of folding of barnase. *FEBS Lett.* 325, 5–16.
- (26) Neira, J. L., and Fersht, A. R. (1996) An NMR study on the β -hairpin region of barnase. *Folding Des.* 1, 231–241.
- (27) Munoz, V., Ghirlando, R., Blanco, F. J., Jas, G. S., Hofrichter, J., and Eaton, W. A. (2006) Folding and aggregation kinetics of a β -hairpin. *Biochemistry* 45, 7023–7035.
- (28) Olsen, K. A., Fesinmeyer, R. M., Stewart, J. M., and Andersen, N. H. (2005) Hairpin folding rates reflect mutations within and remote from the turn region. *Proc. Natl. Acad. Sci. U.S.A.* 102, 15483–15487.
- (29) Du, D., Zhu, Y., Huang, C. Y., and Gai, F. (2004) Understanding the key factors that control the rate of β -hairpin folding. *Proc. Natl. Acad. Sci. U.S.A.* 101, 15915–15920.
- (30) Du, D., Tucker, M. J., and Gai, F. (2006) Understanding the mechanism of β -hairpin folding via ϕ -value analysis. *Biochemistry* 45, 2668–2678.
- (31) Snow, C. D., Qiu, L., Du, D., Gai, F., Hagen, S. J., and Pande, V. S. (2004) Trp zipper folding kinetics by molecular dynamics and temperature-jump spectroscopy. *Proc. Natl. Acad. Sci. U.S.A.* 101, 4077–4082.
- (32) Chen, R. P., Huang, J. J., Chen, H. L., Jan, H., Velusamy, M., Lee, C. T., Fann, W., Larsen, R. W., and Chan, S. I. (2004) Measuring the refolding of β -sheets with different turn sequences on a nanosecond time scale. *Proc. Natl. Acad. Sci. U.S.A.* 101, 7305–7310.
- (33) Xu, Y., Purkayastha, P., and Gai, F. (2006) Nanosecond folding dynamics of a three-stranded β -sheet. *J. Am. Chem. Soc.* 128, 15836–15842.
- (34) Xu, Y., Bunagan, M. R., Tang, J., and Gai, F. (2008) Probing the kinetic cooperativity of β -sheet folding perpendicular to the strand direction. *Biochemistry* 47, 2064–2070.
- (35) Haque, T. S., and Gellman, S. H. (1997) Insights on β -hairpin stability in aqueous solution from peptides with enforced type I' and type II' β -turns. *J. Am. Chem. Soc.* 119, 2303–2304.
- (36) de Alba, E., Jimenez, M. A., and Rico, M. (1997) Turn residue sequence determines β -hairpin conformation in designed peptides. *J. Am. Chem. Soc.* 119, 175–183.
- (37) Espinosa, J. F., Munoz, V., and Gellman, S. H. (2001) Interplay between hydrophobic cluster and loop propensity in β -hairpin formation. *J. Mol. Biol.* 306, 397–402.
- (38) Espinosa, J. F., Syud, F. A., and Gellman, S. H. (2002) Analysis of the factors that stabilize a designed two-stranded antiparallel β -sheet. *Protein Sci.* 11, 1492–1505.
- (39) Gunasekaran, K., Ramakrishnan, C., and Balaram, P. (1997) β -Hairpins in proteins revisited: Lessons for de novo design. *Protein Eng.* 10, 1131–1141.
- (40) Blandl, T., Cochran, A. G., and Skelton, N. J. (2003) Turn stability in β -hairpin peptides: Investigation of peptides containing 3:5 type I G1 bulge turns. *Protein Sci.* 12, 237–247.
- (41) Dyer, R. B., Maness, S. J., Peterson, E. S., Franzen, S., Fesinmeyer, R. M., and Andersen, N. H. (2004) The mechanism of β -hairpin formation. *Biochemistry* 43, 11560–11566.
- (42) Espinosa, J. F., and Gellman, S. H. (2000) A Designed β -Hairpin Containing a Natural Hydrophobic Cluster. *Angew. Chem., Int. Ed.* 39, 2330–2333.
- (43) Constantine, K. L., Mueller, L., Andersen, N. H., Tong, H., Wandler, C. F., Friedrichs, M. S., and Brucoleri, R. E. (1995) Structural and Dynamic Properties of a β -Hairpin-Forming Linear Peptide. 1. Modeling Using Ensemble-Averaged Constraints. *J. Am. Chem. Soc.* 117, 10841–10854.
- (44) de Alba, E., Rico, M., and Jimenez, M. A. (1997) Cross-strand side-chain interactions versus turn conformation in β -hairpins. *Protein Sci.* 6, 2548–2560.
- (45) Searle, M. S., Williams, D. H., and Packman, L. C. (1995) A short linear peptide derived from the N-terminal sequence of ubiquitin folds into a water-stable non-native β -hairpin. *Nat. Struct. Biol.* 2, 999–1006.
- (46) Ramirez-Alvarado, M., Blanco, F. J., and Serrano, L. (1996) De novo design and structural analysis of a model β -hairpin peptide system. *Nat. Struct. Biol.* 3, 604–612.
- (47) Maynard, A. J., Sharman, G. J., and Searle, M. S. (1998) Origin of β -hairpin stability in solution: Structural and thermodynamic analysis of the folding of model peptide supports hydrophobic stabilization in water. *J. Am. Chem. Soc.* 120, 1996–2007.
- (48) Griffiths-Jones, S. R., Maynard, A. J., and Searle, M. S. (1999) Dissecting the stability of a β -hairpin peptide that folds in water: NMR and molecular dynamics analysis of the β -turn and β -strand contributions to folding. *J. Mol. Biol.* 292, 1051–1069.
- (49) de Alba, E., Blanco, F. J., Jimenez, M. A., Rico, M., and Nieto, J. L. (1995) Interactions responsible for the pH dependence of the β -hairpin conformational population formed by a designed linear peptide. *Eur. J. Biochem.* 233, 283–292.
- (50) Kiehna, S. E., and Waters, M. L. (2003) Sequence dependence of β -hairpin structure: Comparison of a salt bridge and an aromatic interaction. *Protein Sci.* 12, 2657–2667.
- (51) Fesinmeyer, R. M., Hudson, F. M., and Andersen, N. H. (2004) Enhanced hairpin stability through loop design: The case of the protein G B1 domain hairpin. *J. Am. Chem. Soc.* 126, 7238–7243.
- (52) Huyghues-Despointes, B. M., Qu, X., Tsai, J., and Scholtz, J. M. (2006) Terminal ion pairs stabilize the second β -hairpin of the B1 domain of protein G. *Proteins* 63, 1005–1017.
- (53) Davis, C. M., Xiao, S., Raleigh, D. P., and Dyer, R. B. (2012) Raising the Speed Limit for β -Hairpin Formation. *J. Am. Chem. Soc.* 134, 14476–14482.
- (54) Blanco, F. J., Rivas, G., and Serrano, L. (1994) A short linear peptide that folds into a native stable β -hairpin in aqueous solution. *Nat. Struct. Biol.* 1, 584–590.
- (55) Kobayashi, N., Endo, S., and Muneakata, E. (1993) Conformational study on the IgG binding domain of protein G. In *Peptide Chemistry 1992* (Yanaikara, N., Ed.) pp 278–281, ESCOM, Leiden, The Netherlands.
- (56) Cochran, A. G., Skelton, N. J., and Starovasnik, M. A. (2001) Tryptophan zippers: Stable, monomeric β -hairpins. *Proc. Natl. Acad. Sci. U.S.A.* 98, 5578–5583.
- (57) Munoz, V., Thompson, P. A., Hofrichter, J., and Eaton, W. A. (1997) Folding dynamics and mechanism of β -hairpin formation. *Nature* 390, 196–199.
- (58) Olsen, K. A. (2006) NMR Studies Reveal the Kinetics and Thermodynamics of Hairpin Formation. Ph.D. Thesis, University of Washington, Seattle.
- (59) Myers, J. K., and Oas, T. G. (2001) Preorganized secondary structure as an important determinant of fast protein folding. *Nat. Struct. Biol.* 8, 552–558.

- (60) Arora, P., Oas, T. G., and Myers, J. K. (2004) Fast and faster: A designed variant of the B-domain of protein A folds in 3 μ s. *Protein Sci.* 13, 847–853.
- (61) Huang, G. S., and Oas, T. G. (1995) Submillisecond folding of monomeric λ repressor. *Proc. Natl. Acad. Sci. U.S.A.* 92, 6878–6882.
- (62) Wang, M., Tang, Y., Sato, S., Vugmeyster, L., McKnight, C. J., and Raleigh, D. P. (2003) Dynamic NMR line-shape analysis demonstrates that the villin headpiece subdomain folds on the microsecond time scale. *J. Am. Chem. Soc.* 125, 6032–6033.
- (63) Andersen, N. H., Olsen, K. A., Fesinmeyer, R. M., Tan, X., Hudson, F. M., Eidenschink, L. A., and Farazi, S. R. (2006) Minimization and optimization of designed β -hairpin folds. *J. Am. Chem. Soc.* 128, 6101–6110.
- (64) Piatto, M., Saudek, V., and Sklenar, V. (1992) Gradient-tailored excitation for single-quantum NMR spectroscopy of aqueous solutions. *J. Biomol. NMR* 2, 661–665.
- (65) Braunschweiler, L., and Ernst, R. R. (1983) Coherence Transfer by Isotropic Mixing: Application to Proton Correlation Spectroscopy. *J. Magn. Reson.* 53, 521–528.
- (66) Fesinmeyer, R. M., Hudson, F. M., Olsen, K. A., White, G. W., Euser, A., and Andersen, N. H. (2005) Chemical shifts provide fold populations and register of β -hairpins and β -sheets. *J. Biomol. NMR* 33, 213–231.
- (67) Piette, L. H., and Anderson, W. A. (1959) Potential Energy Barrier Determinations for Some Alkyl Nitrites by Nuclear Magnetic Resonance. *J. Chem. Phys.* 30, 899–908.
- (68) de Alba, E., Santoro, J., Rico, M., and Jimenez, M. A. (1999) De novo design of a monomeric three-stranded antiparallel β -sheet. *Protein Sci.* 8, 854–865.
- (69) Ferguson, N., Sharpe, T. D., Schartau, P. J., Sato, S., Allen, M. D., Johnson, C. M., Rutherford, T. J., and Fersht, A. R. (2005) Ultra-fast barrier-limited folding in the peripheral subunit-binding domain family. *J. Mol. Biol.* 353, 427–446.
- (70) Ferguson, N., Sharpe, T. D., Johnson, C. M., Schartau, P. J., and Fersht, A. R. (2007) Structural biology: Analysis of “downhill” protein folding. *Nature* 445, E14–E15 E17–E18 (discussion).
- (71) Kier, B. L., and Andersen, N. H. (2008) Probing the lower size limit for protein-like fold stability: Ten-residue microproteins with specific, rigid structures in water. *J. Am. Chem. Soc.* 130, 14675–14683.
- (72) Eidenschink, L., Kier, B. L., Huggins, K. N., and Andersen, N. H. (2009) Very short peptides with stable folds: Building on the interrelationship of Trp/Trp, Trp/cation, and Trp/backbone-amide interaction geometries. *Proteins* 75, 308–322.
- (73) Kier, B. L., Shu, I., Eidenschink, L. A., and Andersen, N. H. (2010) Stabilizing capping motif for β -hairpins and sheets. *Proc. Natl. Acad. Sci. U.S.A.* 107, 10466–10471.
- (74) Shu, I., Scian, M., Kier, B. L., Williams, D. H., and Andersen, N. H. (2010) Tryptophan interactions that stabilize folding motifs: a guide to placement, dynamics, and optimizing fold stabilization. In *Proceedings of the 31st European Peptide Symposium* (Lebl, M., Meldal, M., Jensen, K. J., and Hoeg-Jensen, T., Eds.) pp 614–615, European Peptide Society, Prato, Via Francesco, Italy.
- (75) Honda, S., Yamasaki, K., Sawada, Y., and Morii, H. (2004) 10 residue folded peptide designed by segment statistics. *Structure* 12, 1507–1518.
- (76) Honda, S., Akiba, T., Kato, Y. S., Sawada, Y., Sekijima, M., Ishimura, M., Ooishi, A., Watanabe, H., Odahara, T., and Harata, K. (2008) Crystal structure of a ten-amino acid protein. *J. Am. Chem. Soc.* 130, 15327–15331.
- (77) Nguyen, H., Jager, M., Kelly, J. W., and Gruebele, M. (2005) Engineering a β -sheet protein toward the folding speed limit. *J. Phys. Chem. B* 109, 15182–15186.
- (78) Liu, F., Du, D., Fuller, A. A., Davoren, J. E., Wipf, P., Kelly, J. W., and Gruebele, M. (2008) An experimental survey of the transition between two-state and downhill protein folding scenarios. *Proc. Natl. Acad. Sci. U.S.A.* 105, 2369–2374.
- (79) Fuller, A. A., Du, D., Liu, F., Davoren, J. E., Bhabha, G., Kroon, G., Case, D. A., Dyson, H. J., Powers, E. T., Wipf, P., Gruebele, M., and Kelly, J. W. (2009) Evaluating β -turn mimics as β -sheet folding nucleators. *Proc. Natl. Acad. Sci. U.S.A.* 106, 11067–11072.
- (80) Shu, I. (2011) Thermodynamics and Kinetics of β -Sheet Folding Models. Ph.D. Thesis, University of Washington, Seattle.
- (81) Krieger, F., Fierz, B., Bieri, O., Drewello, M., and Kiefhaber, T. (2003) Dynamics of unfolded polypeptide chains as model for the earliest steps in protein folding. *J. Mol. Biol.* 332, 265–274.
- (82) Krieger, F., Moglich, A., and Kiefhaber, T. (2005) Effect of proline and glycine residues on dynamics and barriers of loop formation in polypeptide chains. *J. Am. Chem. Soc.* 127, 3346–3352.
- (83) Kubelka, J., Hofrichter, J., and Eaton, W. A. (2004) The protein folding “speed limit”. *Curr. Opin. Struct. Biol.* 14, 76–88.
- (84) Dyer, R. B. (2007) Ultrafast and downhill protein folding. *Curr. Opin. Struct. Biol.* 17, 38–47.